Spectrochimica Acta Part A: Molecular and Biomolecular Spectroscopy 104 (2013) 358–367

Contents lists available at SciVerse ScienceDirect

Spectrochimica Acta Part A: Molecular and Biomolecular Spectroscopy

journal homepage: www.elsevier.com/locate/saa

Vibrational spectroscopy and density functional theory analysis of 3-*O*-caffeoylquinic acid

Soni Mishra [a], Poonam Tandon [b,*], Pinkie J. Eravuchira [c], Rasha M. El-Abassy [d], Arnulf Materny [d]

[a] Department of Inorganic and Physical Chemistry, Indian Institute of Science, Bangalore 560 012, India
[b] Department of Physics, University of Lucknow, Lucknow 226 007, India
[c] EMaS Universitat Rovira I Virgili, Tarragona, Spain
[d] Chemical Physics, Jacobs University Bremen, Campus Ring 1, 28759 Bremen, Germany

HIGHLIGHTS

- Infrared and Raman spectra were recorded and compared with the theoretical results.
- The complete assignments are performed on the basis of the potential energy distribution.
- The theoretical calculations were made using B3LYP/6-311G(d,p) method.
- Stability of the molecule has been analyzed using natural bond orbital analysis.
- The HOMO and LUMO energies show that charge transfer occurs within the molecule.

GRAPHICAL ABSTRACT

Comparison of the optimized structures of the regioisomers of chlorogenic acid.

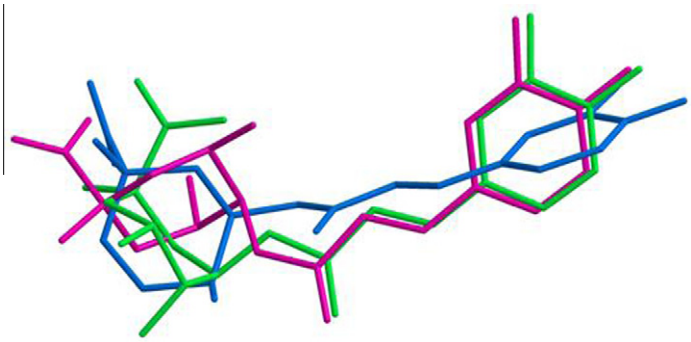

ARTICLE INFO

Article history:
Received 3 November 2012
Received in revised form 19 November 2012
Accepted 23 November 2012
Available online 5 December 2012

Keywords:
Raman spectroscopy
Chlorogenic acid
Vibrational analysis
DFT
NBO

ABSTRACT

Density functional theory (DFT) calculations are being performed to investigate the geometric, vibrational, and electronic properties of the chlorogenic acid isomer 3-CQA (1R,3R,4S,5R)-3-{[(2E)-3-(3,4-dihydroxyphenyl)prop-2-enoyl]oxy}-1,4,5-trihydroxycyclohexanecarboxylic acid), a major phenolic compound in coffee. DFT calculations with the 6-311G(d,p) basis set produce very good results. The electrostatic potential mapped onto an isodensity surface has been obtained. A natural bond orbital analysis (NBO) has been performed in order to study intramolecular bonding, interactions among bonds, and delocalization of unpaired electrons. HOMO–LUMO studies give insights into the interaction of the molecule with other species. The calculated HOMO and LUMO energies indicate that a charge transfer occurs within the molecule.

Introduction

Chlorogenic acids are a family of esters formed between certain trans-cinnamic acids and quinic acid (1L-1 (OH),3,4/5-tetrahydroxycyclohexane carboxylic acid), which has axial hydroxyls on carbons 1 and 3 and equatorial hydroxyls on carbons 4 and 5. During processing, *trans* isomers may be partially converted to *cis*. Chlorogenic acids belong to the group of phenols and are found in coffee as well as many other plants.

Prunes are well-known as healthy food and have been used medically in India in combination with other drugs for the treatment of leukorrhoea, irregular menstruation, and debility following miscarriage [1]. It is reported that neochlorogenic acid (3-*O*-caffeoylquinic acid, 3-CQA) is a major hydroxycinnamate

* Corresponding author. Tel.: +91 522 2782653; fax: +91 522 2740840.
E-mail addresses: poonam_tandon@hotmail.com, poonam_tandon@yahoo.co.uk (P. Tandon).

1386-1425/$ - see front matter © 2012 Elsevier B.V. All rights reserved.
http://dx.doi.org/10.1016/j.saa.2012.11.082

(541 mg/kg) in the plum fruit. Chlorogenic acid (5-*O*-caffeoylquinic acid, 5-CQA) is also contained at a concentration of 73 mg/kg, and cryptochlorogenic acid (4-*O*-caffeoylquinic acid, 4-CQA) was found at 9 mg/kg as a minor component [2]. Neochloroenic acid could be involved in the laxative effect observed in prunes. Dried prunes contain higher amounts of phenolic compounds. Neochlorogenic acid represents 71% of the total phenolics and chlorogenic acid 24%, raising the content of hydroxycinnamates to 95% of all phenolic compounds [3]. Chlorogenic acid, 5-CQA, is widely recognized as an antioxidant for human LDL (low-density lipoprotein) [4,5]. It is also known as a scavenger for reactive species of oxygen and nitrogen [6] and an inhibitor against formation of conjugated diene from linoleic acid oxidation [7].

As already mentioned above, chlorogenic acid is a major phenolic compound in coffee. Therefore, coffee is an important source of chlorogenic acid in the human diet; daily intake in coffee drinkers is 0.5–1 g; coffee abstainers will usually ingest <100 mg/d. Other dietary sources of chlorogenic acid include apples, pears, berries, artichoke, and aubergine [8], or the above mentioned plums. Chlorogenic acid and caffeic acid are antioxidants in vitro [9,10] and might therefore contribute to the prevention of cardiovascular disease [11]. It is also believed that they can inhibit the formation of mutagenic and carcinogenic N-nitroso compounds because they are inhibitors of the N-nitrosation reaction in vitro [12]. The absorbed fraction of chlorogenic acid will enter into the blood circulation and thus can induce biological effects in the blood circulation. Therefore, a better understanding of the effect of chlorogenic acids in humans is essential to evaluate possible health effects *in vivo*.

In continuation to our work on Raman spectroscopic studies of different regioisomers of monoacyl and diacyl chlorogenic acid [13], in the present communication, we report systematic study of the geometrical structure and electrostatic potential surfaces of 3-CQA (Fig. 1) based on vibrational spectroscopy results and density functional theory (DFT) computations. Geometry optimizations of the 3-CQA, 4-CQA, and 5-CQA regioisomers were performed, and the corresponding relative energies were compared. We have calculated the equilibrium geometry, harmonic vibrational wavenumbers, electrostatic potential surfaces, absolute Raman scattering activities and infrared absorption intensities by DFT with B3LYP functionals having the extended basis set 6-311G(d,p). The calculated vibrational spectra have been analyzed on the basis of the potential energy distribution (PED) of each vibrational mode, which allowed us to obtain a quantitative as well as qualitative interpretation of the infrared and Raman spectra. The natural bonding orbitals (NBO) analysis has been performed in order to investigate intramolecular charge transfer interactions, rehybridization and delocalization of electron density within the molecule. IR and Raman spectroscopic studies along with HOMO and LUMO analysis have been used to elucidate information regarding charge transfer within the molecule.

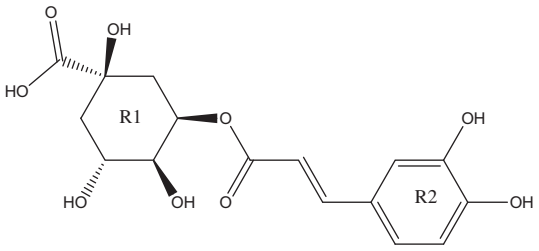

Fig. 1. Chemical structure of 3-CQA.

Experimental details

Pure samples of the caffeoylquinic acids were purchased from PhytoLab. All samples were white solid powders. Their purity was assessed using HPLC–MS. Raman experiments were performed using a microRaman setup, which includes an Argon Ion laser source emitting at 514.5 nm. The spectral resolution of the micro Raman setup is 3 cm^{-1}. The laser was focused into the CGA samples with an excitation power of 5 mW at the sample. Both the focusing of the excitation laser into the sample and the collection of the scattered light from the sample were done with the help of a microscope equipped with a 100× ultra long working distance objective (N.A. 0.90, Olympus).

Infrared spectra were recorded on a Bruker IFS28 FT-IR spectrometer with a spectral resolution of 4 cm^{-1}. KBr pellets of solid samples were prepared from mixtures of 200 mg KBr with 2 mg of sample in a laboratory press.

Computational details

The DFT calculations are being performed with the Gaussian03 program [14] and are analyzed with the help of the GaussView program [15]. All calculations were carried out at the density functional level of theory employing the Becke's three parameter (local, nonlocal, Hartree–Fock) hybrid exchange functionals with Lee–Yang–Parr correlation functionals (B3LYP) [16–18] and the basis set 6-311G(d,p) augmented by 'd' polarization functions on heavy atoms and 'p' polarization functions on hydrogen atoms as well as diffuse functions for both hydrogen and heavy atoms were used [19,20]. The absolute Raman and IR absorption intensities were calculated in the harmonic approximation, at the same level of theory as used for optimized geometries, from the derivatives of the dipole moment and polarizability of each normal mode, respectively. Recently some interesting papers using uniform scaling, shows very good agreement between calculated and experimental frequencies [21,22]. In addition to uniform frequency scaling factors, dual scaling factors were determined to improve the agreement between computed and observed frequencies. The dual scaled error distributions are more symmetric, compared with the uniform scaled frequency errors. The vibrational wavenumbers were obtained from the DFT calculations using a dual scaling procedure for the fingerprint region (below 1800 cm^{-1}) and X—H stretching (above 1800 cm^{-1}) regions, respectively [23,24]. Raman and IR spectra were simulated using a Lorentzian line shape with a FWHM (full width at half maximum) of 8 cm^{-1} for each peak. The normal mode analysis was performed, and the PED was calculated for each internal coordinates using localized symmetry [25,26]. For this purpose, a complete set of internal coordinates was defined for both forms using Pulay's recommendations [25,26]. All calculations were performed with the Gaussian 03 package [14]. The vibrational assignments of the normal modes were proposed on the basis of the PED calculated using program GAR2PED [27]. For the visualization and correlation of calculated data we have used CHEMCRAFT [28] and Gauss View [15].

The main natural orbital interactions were analyzed on the basis of NBO calculations done at DFT/B3LYP level using the NBO 5.0 program as implemented in the Gaussian 03 package. In the NBO analysis [29,30] the electronic wave functions are interpreted in terms of a set of occupied Lewis-type (bond or lone pair) and a set of unoccupied non-Lewis (antibond or Rydberg) localized NBO orbitals. The delocalization of electron density (ED) between these orbitals corresponds to a stabilizing donor–acceptor interaction. Second-order perturbation theory has been employed to evaluate the stabilization energies of all possible interactions between

donor and acceptor orbitals in the NBO basis. The interactions result in a loss of occupancy from the localized NBO of the idealized Lewis structure into an empty non-Lewis orbital. The delocalization effects (or donor–acceptor charge transfers (CTs)) can be estimated from off-diagonal elements of the Fock matrix in the NBO basis. For each donor (i) and acceptor (j), the stabilization energy $E^{(2)}$ associated with the delocalization $i \rightarrow j$ is estimated as

$$E^{(2)} = \Delta E_{ij} = q_i \frac{F(i,j)^2}{\varepsilon_j - \varepsilon_i}$$

where q_i is the donor orbital occupancy, ε_i and ε_j are diagonal elements and $F(i,j)$ is the off-diagonal NBO Fock or Kohn–Sham matrix element [29].

Results and discussions

Geometry optimizations

The optimized structure parameters of 3-CQA, 4-CQA, and 5-CQA (Fig. 2) were calculated by DFT (B3LYP) level with the 6-311G(d,p) basis set. Fig. 2 clearly shows that the cyclohexane and the phenyl ring assume *trans* configuration with respect to the ethylenic C18═C19 bond. The position of the cyclohexane ring is different in all the chlorogenic acids. 3-CQA (−1297.924 Hartree) is more stable than 5-CQA (−1297.922 Hartree) and 4-CQA (−1297.908 Hartree). The energy difference between 3-CQA and 5-CQA is 1.255 kcal mol^{-1}, and that between 3-CQA and 4-CQA is 10.040 kcal mol^{-1} for the basis set 6-311G(d,p). Selected physical parameters have been calculated and are listed in Table 1. Theoretically computed energies (arb. units), zero-point vibrational energies (kcal mol^{-1}), entropies (cal mol^{-1} K^{-1}), and dipole moment (Debyes) for 3-CQA, 4-CQA and 5-CQA are also listed in Table 1.

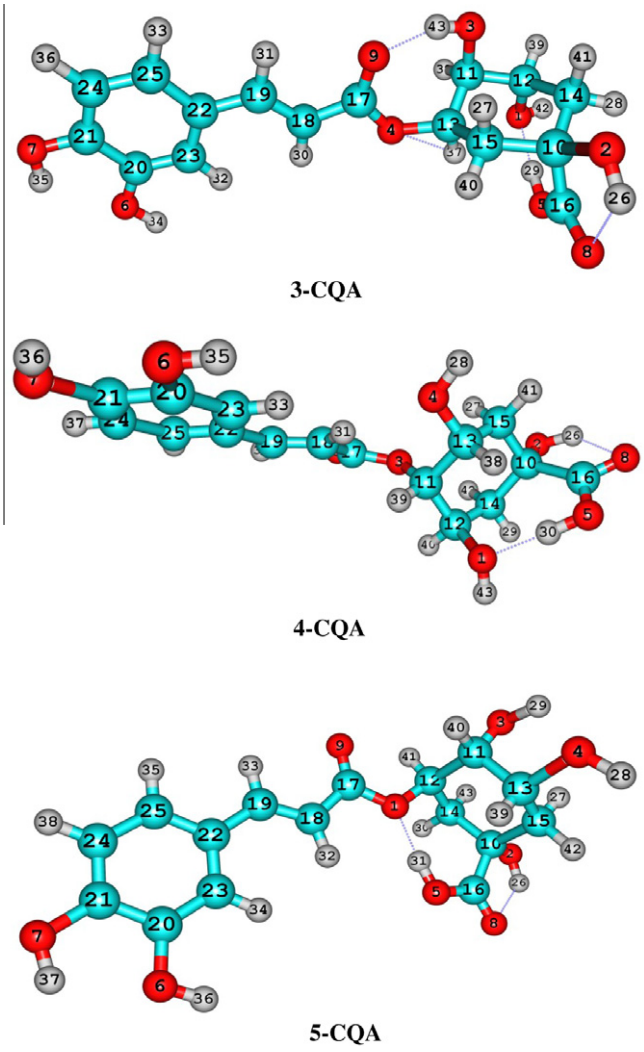

Fig. 2. Optimized structures of 3-CQA, 4-CQA and 5-CQA.

Table 1
Theoretically computed energies (arb. units), zero point vibratonal energies (kcal mol^{-1}) rotational constants (GHz), entropies (cal mol^{-1} K^{-1}) and dipole moment (Debyes).

Parameters	3-CQA	4-CQA	5-CQA
Total energy	−1297.92419	−1297.90799	−1297.92229
Zero-point energy	211.02	210.42	210.52
Rotational constants			
	0.5304	0.5068	0.4210
	0.0687	0.0807	0.0831
	0.0664	0.0751	0.0753
Entropy			
Total	163.173	165.505	167.123
Translational	43.487	43.487	43.487
Rotational	36.140	35.903	36.056
Vibrational	83.546	86.115	87.580
Dipole moment	4.757	5.784	4.675

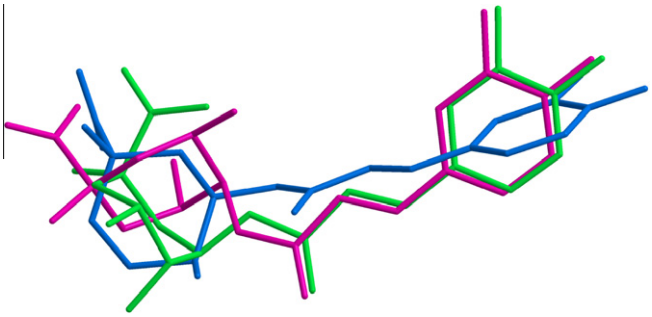

Fig. 3. Comparison of the optimized structures of the 3-CQA (pink), 4-CQA (blue) and 5-CQA (green) isomers. (For interpretation of the references to color in this figure legend, the reader is referred to the web version of this article.)

In 3-CQA, there exists the possibility of four stronger intramolecular hydrogen bonds OH···O owing to a smaller distance of less than 2 Å between atoms H and O. In 5-CQA and 4-CQA, there are only two stronger intramolecular hydrogen bonds owing to a smaller distance of 1.68 and 1.96 Å. The optimized structures of the 3-CQA, 4-CQA, and 5-CQA molecule were compared by superimposing them using a least-squares algorithm that minimizes the distances between the corresponding non-hydrogen atoms (Fig. 3). The agreement between these molecules is showing that the geometry optimization almost reproduces the different conformations (overall average deviation 0.078 Å). The main differences are due to the misorientation of cyclohexane ring.

Molecular electrostatic potential

The molecular electrostatic potential (MEP) is a powerful tool that provides insights into intermolecular association and molecular properties of small molecules, actions of drug molecules and their analogs, the biological function of hemoglobin, and enzyme catalysis [31–34]. MEP is widely used as a reactivity map displaying most probable regions for the electrophilic attack of charged point-like reagents on organic molecules [31]. The values and spatial distribution of MEP are in fact responsible for the chemical behavior of an agent in a chemical reaction. They strongly influence the binding of a substrate to its active site. MEP is typically

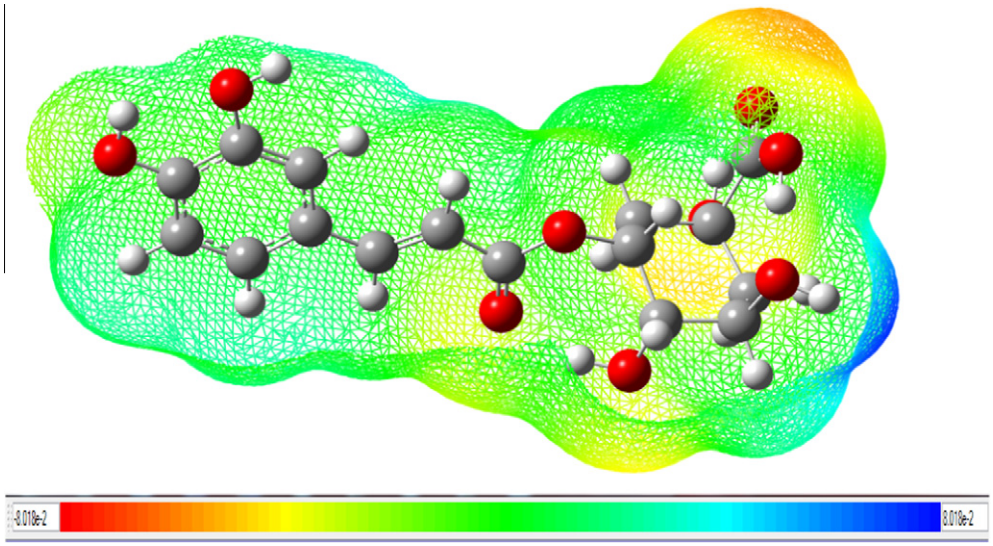

Fig. 4. Molecular electrostatic potential mapped on the isodensity surface in the range from -8.018×10^{-2} (red) to $+8.018 \times 10^{-2}$ (blue) for 3-CQA. (For interpretation of the references to color in this figure legend, the reader is referred to the web version of this article.)

Table 2
Second order perturbation theory analysis of Fock matrix in NBO basis of 3-CQA.

Donor NBO(i)	*ED*(*i*) (e)	Acceptor *NBO(j)*	*ED*(*j*) (e)	$E^{(2)}$ [a] (kcal mol^{-1})	$E(j) - E(i)$[b](arb.u.)	$F(i,j)$[c] (arb.u.)
n2(O1)	1.92549	σ*O5—H29	0.05950	23.26	0.85	0.126
n2(O2)	1.94578	σ*C10—C15	0.04080	8.29	0.63	0.065
n2(O3)	1.94533	σ*C11—H38	0.03871	10.14	0.69	0.075
n2(O4)	1.78996	π*O9—C17	0.30829	44.90	0.33	0.112
n2(O5)	1.79284	π*O8—C16	0.21216	44.71	0.36	0.113
n2(O6)	1.89188	π*C20—C23	0.35326	25.59	0.36	0.092
n2(O7)	1.85201	π*C21—C24	0.37234	30.29	0.35	0.097
n2(O8)	1.84185	σ*O5—C16	0.08097	28.38	0.66	0.124
n2(O9)	1.84418	σ*O4—C17	0.09429	26.81	0.65	0.120
πO5—H29	1.98457	σ*O8—C16	0.02775	4.46	1.36	0.070
πO7—H35	1.98749	σ*C21—C24	0.02299	4.89	1.30	0.071
πC14—H41	1.96243	σ*O1—C12	0.03282	5.92	0.72	0.058
πC18—C19	1.84206	π*O9—C17	0.30829	23.63	0.26	0.076
		π*C22—C25	0.39930	11.10	0.30	0.055
πC20—C23	1.72610	π*C21—C24	0.37234	18.07	0.30	0.067
		π*C22—C25	0.39930	16.84	0.31	0.065
πC21—C24	1.64589	π*C20—C23	0.35326	19.44	0.28	0.066
		π*C22—C25	0.39930	21.94	0.29	0.072
πC22—C23	1.96723	σ*O6—C20	0.02368	4.74	1.01	0.062
πC22—C25	1.64151	π*C18—C19	0.13409	19.36	0.28	0.071
		π*C20—C23	0.35326	20.15	0.26	0.066
		π*C21—C24	0.37234	19.21	0.27	0.065
π*O9—C17	0.30829	π*C18—C19	0.13409	46.41	0.03	0.074
π*C20—C23	0.35326	π*C22—C25	0.39930	264.41	0.01	0.079

[a] $E(2)$ is the energy of hyperconjugative interactions.
[b] Energy difference between donor and acceptor i and j NBO orbitals.
[c] $F(i,j)$ is the Fock matrix element between i and j NBO orbitals.

visualized through mapping its values onto the molecular electron density. The different values of the electrostatic potential at the surface are represented by different colors; red represents regions of the most negative electrostatic potential, blue represents regions of the most positive electrostatic potential and green represents regions of zero potential. The potential increases in the order red < orange < yellow < green < blue. While the negative electrostatic potential corresponds to an attraction of the proton by the concentrated electron density in the molecule (and is colored in shades of red), the positive electrostatic potential corresponds to repulsion of the proton by atomic nuclei in regions where low electron density exists and the nuclear charge is incompletely shielded (and is colored in shades of blue). The molecular electrostatic potential map (MEP) for 3-CQA is shown in Fig. 4. The MEP plot of 3-CQA reveals major active centers at oxygen atoms of the hydroxyl group of rings and of the carboxylic acid group characterized by red color. The oxygen atoms of the hydroxyl and the carboxylic group represent the most negative potential region and have an excess of negative charge (red region) and the hydrogen atoms bear the positive charge (blue region). The predominance of green color on the remaining part of the molecule including the bromine atom attached to the ring indicates a neutral potential.

Natural bond orbital analysis

NBO analysis proves to be an efficient method for the study of the intra- and intermolecular bonding and interactions among

Table 3
Theoretical and experimental vibrational wavenumbers (cm^{-1}) of isomers of chlorogenic acid.

3CQA		4CQA scaled	5CQA scaled	Raman	Ref. [37]	IR	Assignment
Unscaled	scaled			3CQA		3CQA	
3848	3716	3716	3715	–	–	–	ν(O6H)(100)
3844	3713	3705	3705	–	–	–	ν(O1H)(79) + oop(O1—H)(21)
3778	3649	3703	3660	–	–	–	ν(O7H)(100)
3684	3559	3651	3647	–	–	–	ν(O2H)(99)
3577	3455	3558	3571	–	–	3421	ν(O3H)(100)
3345	3231	3250	3344	–	–	–	ν(O5H)(100)
3201	3092	3110	3092	3108	–	–	R2[ν(CH)](99)
3198	3089	3090	3080	3080	–	–	ν(C18H)(97)
3180	3071	3070	3071		–	–	R2[ν(C25H)](98)
3164	3056	3055	3058	3048	–	–	R2[ν(CH)](98)
3153	3045	3046	3045	3041	–	–	ν(C19H)(97)
3124	3017	2997	3013	–	–	–	$\nu(C15H_2)(92)$ + ν(C13—H)(7)
3107	3001	2994	3001	–	–	–	$\nu(C14H_2)(99)$
3095	2990	2977	2992	–	–	–	ν(C13—H)(91) + $\nu(C15H_2)(8)$
3071	2966	2964	2957	–	–	–	ν(C12—H)(94) + $\nu(C14H_2)(5)$
3061	2956	2942	2929	–	–	–	$\nu(C15H_2)(80)$ + $\nu(C15H_2)(19)$
3046	2942	2930	2916	–	–	2937	$\nu(C14H_2)(94)$
2992	2890	2901	2904	2989	–		ν(C11—H)(99)
1809	1719	1784	1783	–	–	1726	ν(C16═O)(75) + ρ(C16OO)(7) + δ(CO5H)(6) + ν(C—O5)(5)
1731	1747	1749	1750	–	1688	–	ν(C17═O)(48) + ρ(CC17O)(19) + δ(CC17O)(14) + ν(C18═C19)(5)
1673	1661	1660	1662	1680	–	1686	ν(C18═C19)(32) + R2[ν_{ring}](19) + ρ(CC19H)(7) + ν(C17—C18)(7) + ν(C17═O)(6)
1642	1630	1633	1631	1627	1629	1639	R2[ν_{ring}](21) + ν(C18═C19)(15) + ν(C19—C22)(7) + ρ(CC23H)(5)
1635	1623	1623	1622	1605		1612	R2[ν_{ring}](65) + R2[δ_{ring}](10) + δ(CO7H)(7) + ρ(CC25H)(6) + δ(CCO7)(5)
1559	1547	1547	1548	–	1518	1527	R2[ν_{ring}](38) + ρ(CC23H)(14) + ν(C—O7)(11) + ρ(CC24H)(10) + ρ(CC25H)(9)
1500	1489	1486	1481	–		1487	$\delta(C15H_2)(87)$ + $\delta(C14H_2)(6)$
1483	1472	1470	1472	–	1474	–	R2[ν_{ring}](48) + ρ(CC24H)(8) + ν(C—O6)(8) + ρ(CC25H)(8)
1476	1466	1464	1462	1472	–	–	$\delta(C14H_2)(39)$ + δ(CO3H)(15) + δ(HC13O)(8) + ρ(C13—O)(6) + ω(C11O)(6)
1467	1457	1445	1440	–	–	–	δ(CO3H)(22) + $\delta(C14H_2)(19)$ + δ(HC13O)(10) + ρ(C13—O)(7) + ω(C11O)(7) + δ(CO5H)(5) + $\delta(C15H_2)(5)$
1457	1446	1436	1437	1444	–	1443	δ(CO5H)(37) + $\delta(C14H_2)(16)$ + δ(CO2H)(15) + ν(C—O5)(8) + ν(C10—C16)(5)
1446	1435	1411	1414	–			δ(HC13O)(49) + ρ(C13—O)(19) + δ(CO3H)(10)
1426	1415	1409	1412	–	1444	1419	δ(CO2H)(29) + δ(CO5H)(24) + ω(C12O)(6) + R1[ν_{ring}](5)
1420	1410	1407	1401	–	1382	–	R2[ν_{ring}](40) + δ(CO7H)(26) + ρ(CC25H)(6)
1406	1396	1399	1397	–	–	–	δ(HC12O)(29) + δ(CO1H)(20) + ρ(C12O)(11) + oop(O1—H)(9)
1398	1387	1374	1375	–	–	1385	δ(HC11O)(13) + ω(C13—O)(12) + γ(C13—O)(10) + ω(C11O)(10) + γ(C11O)(7) + δ(CO1H)(7) + oop(C13—H)(6) + δ(HC12O)(5) + ρ(C11O)(5)
1378	1368	1364	1365	1370	–	–	$\omega(C14H_2)(33)$ + ω(C12O)(11) + γ(C12O)(7) + δ(HC12O)(6) + ρ(C12O)(6) + δ(CO5H)(5)
1363	1353	1354	1355	–	–	1358	ρ(CC19H)(20) + ρ(CC25H)(12) + R2[ν_{ring}](11) + δ(CO6H)(9) + δ(CO7H)(8) + ρ(CC24H)(8) + ρ(CC18H)(7) + ρ(CC23H)(5) + ν(C17—C18)(5)
1354	1344	1352	1349	–	1344	1340	ω(C12O)(13) + R1[ν_{ring}](11) + $\omega(C14H_2)(7)$ + γ(C12O)(6) + $\omega(C15H_2)(6)$ + ω(C11O)(6) + ω(C13—O)(5) + δ(CO3H)(5) + γ(C11O)(5)
1347	1337	1343	1334	–	–	–	ρ(CC18H)(15) + R2[ν_{ring}](10) + ν(C19—C22)(9) + ν(C17—C18)(8) + R2[ν_{ring}](8) + ν(C17—O4)(6) + R2[ν_{ring}](6) + δ(CC17O)(5)
1337	1327	1325	1330	–	–	1323	R2[ν_{ring}](21) + ρ(CC19H)(19) + ν(C18═C19)(10) + ν(C19—C22)(7) + ρ(CC18H)(6) + δ(CC19C)(5) + δ(CO6H)(5)
1336	1326	1320	1329	–	–	–	δ(HC11O)(21) + ω(C12O)(11) + R1[ν_{ring}](8) + δ(CO1H)(8) + ρ(C11O)(8) + ω(C13—O)(8) + γ(C13—O)(6) + $\gamma(C15H_2)(5)$
1322	1312	1304	1305	–	–	–	$\omega(C15H_2)(33)$ + $\omega(C14H_2)(8)$ + δ(CO3H)(5)
1312	1302	1287	1304	–	–	1304	ν(C—O7)(41) + ρ(CC23H)(13) + R2[ν_{ring}](13) + R2[δ_{ring}](7)
1288	1279	1274	1278	1285	1287	1288	$\gamma(C14H_2)(26)$ + $\omega(C15H_2)(21)$ + δ(CO2H)(12) + ν(C-O5)(5) + δ(HC12O)(5)
1276	1267	1267	1266	–	–	–	ρ(CC23H)(17) + ρ(CC25H)(14) + ρ(CC19H)(12) + ν(C—O6)(9) + R2[δ_{ring}](9) + ν(C—O7)(7) + δ(CO7H)(5)
1267	1257	1250	1250	1250	1252	1256	ω(C11O)(15) + γ(C11O)(9) + ν(C—O5)(9) + R1[ν_{ring}](8) + $\omega(C14H_2)(8)$ + δ(HC11O)(6) + $\gamma(C15H_2)(5)$
1244	1235	1233	1239	–	–	–	ν(C—O5)(35) + $\gamma(C14H_2)(14)$ + δ(CC16O)(9) + $\gamma(C15H_2)(6)$
1230	1221	1210	1224	–	–	1223	δ(CO1H)(49) + oop(O1—H)(24) + ρ(C12O)(6)
1215	1206	1205	1208	–	1203	1201	R2[ν_{ring}](30) + δ(CO7H)(27) + ρ(CC24H)(13)
1207	1198	1197	1198	–	–	1190	$\gamma(C15H_2)(26)$ + $\gamma(C14H_2)(11)$ + R1[ν_{ring}](9) + ω(C11O)(7)
1193	1185	1181	1182	1183	1188	–	ρ(CC18H)(20) + ν(C17—O4)(18) + δ(CC17O)(8) + ν(C17—C18)(6) + ρ(CC17O)(5) + δ(CO6H)(5)
1183	1175	1162	1163	1167	–	1173	ν(C17—O4)(14) + ρ(CC23H)(13) + ν(C19—C22)(12) + δ(CO6H)(12) + δ(CC17O)(8) + R2[ν_{ring}](6) + ν(C17—C18)(5)
1171	1162	1137	1134	–	1160	1159	δ(CO6H)(26) + R2[ν_{ring}](22) + ρ(CC24H)(20) + ν(C—O6)(15) + ρ(CC25H)(5)
1154	1146	1136	1131	–	–	–	δ(CO1H)(19) + R1[ν_{ring}](19) + oop(O1—H)(11) + ν(C11—O3)(9) + ν(C10—O2)(5) + γ(C13—O)(5)
1139	1131	1122	1122	–	–	1132	R1[$puck_{ring}$](21) + ρ(C10—O)(18) + ν(C10—O2)(12) + $\rho(C15H_2)(7)$ + ρ(C13—O)(6) + ν(C11—O3)(6) + R1[ν_{ring}](10)
1131	1122	1120	1116	1119	1116	–	ρ(CC25H)(18) + R2[δ_{ring}](16) + R2[ν_{ring}](13) + δ(CO6H)(11) + ν(C—O6)(11) + ρ(CC24H)(6)
1118	1109	1113	1114	–	–	–	ν(C10—O2)(18) + R1[ν_{ring}](16) + R1[δ_{ring}](14) + δ(CC10—O)(5) + R1[ν_{ring}](5)
1110	1102	1088	1101	–	–	–	R1[ν_{ring}](30) + δ(CO1H)(18) + ν(C10—O2)(8) + oop(O1—H)(8) + R1[ν_{ring}](7) + ν(C11—O3)(7)
1068	1060	1063	1063	–	–	1084	R1[ν_{ring}](32) + γ(C12O)(16) + $\rho(C14H_2)(5)$ + δ(CO1H)(5)
1047	1039	1058	1046	–	–	1036	ν(C12—O1)(12) + ρ(C13—O)(11) + ν(C11—O3)(11) + ν(C13—O4)(9)
1033	1025	1040	1023	–	–	–	ν(C13—O4)(16) + ν(C17—C18)(10) + ν(C12—O1)(10) + R1[ν_{ring}](9) + ρ(C13—O)(8) + ν(C17—O4)(5) + ν(C11—O3)(5)
1027	1020	1021	1019	–	–	–	ω(C19—H)(54) + τ(C18—C19)(34) + ω(C18—H)(5)
991	984	987	997	–	1000	999	ν(C12—O1)(11) + R2[ν_{ring}](14) + ν(C13—O4)(5) + $\rho(C15H_2)(5)$
989	982	982	982	–	980	978	ν(C12—O1)(15) + $\rho(C15H_2)(9)$ + R1[ν_{ring}](9) + R2[ν_{ring}](8)
955	948	945	967	976	–	–	τ(C—O5)(14) + R1[δ_{ring}](12) + R1[ν_{ring}](9) + ν(C13—O4)((6) + ν(C17—C18)(5) + ρ(C12O)(5)

Table 3 (*continued*)

3CQA		4CQA scaled	5CQA scaled	Raman	Ref. [37]	IR	Assignment
Unscaled	scaled			3CQA		3CQA	
945	938	937	942	–	–	937	R2[oop(C25—H)](46) + R2[oop(C24—H)](40) + R2[puck$_{ring}$](6) + R2[τ_{ring}](5)
935	929	932	937	–	–	–	R1[ν_{ring}](21) + δ(CO1H)(11) + τ(C—O5)(10) + ρ(C15H$_2$)((8) + oop(O1—H)(8)
925	919	918	895	–	–	–	τ(C—O5)(35) + ρ(C14H$_2$)(9) + ρ(C13—O)(6) + R1[τ_{ring}](5) + ρ(C15H$_2$)(5) + oop(O1—H)(5)
921	914	911	890	–	–	908	ν(C13—O4)(16) + R1[ν_{ring}](19) + δ(CO4C)(9) + R1[δ_{ring}](6) + τ(C—O5)(5)
886	879	888	868	–	–	889	ω(C18—H)(47) + ω(C19—H)(15) + oop(C=O9)(12) + τ(C18—C19)(9)
878	872	885	843	854	–	872	ν(C10—C16)(14) + R1[ν_{ring}](26) + ρ(C14H$_2$)(5) + ρ(C10—O)(5)
843	837	848	835	–	858	839	R2[oop(C23—H)](53) + R2[oop(C25—H)](14) + R2[τ_{ring}](7) + R2[oop(C24—H)](7) + R2[puck$_{ring}$](7) + oop(C22—C19)(5)
842	836	841	819	–	821	–	ν(C12—O1)(17) + R1[ν_{ring}](23) + ρ(C14H$_2$)(13) + ρ(C10—O)(7) + ρ(C11O)(5) + R1[τ_{ring}](5)—R1[δ_{ring}](5)
826	820	821	817	817	–	818	R2[oop(C24—H)](31) + R2[oop(C23—H)](26) + R2[oop(C25—H)](18) + R2[puck$_{ring}$](8) + oop(C—O7)(5) + ω(C20—O)(5)
816	810	808	800	–	–	806	R2[δ_{ring}](28) + ν(C—O7)(17) + R2[ν_{ring}](16) + ρ(CC17O)(6)
789	784	781	787	–	–	–	ρ(CC17O)(18) + δ(CO4C)(14) + ω(C=O8)(5) + ρ(C16OO)(5) + δ(CC17O)(5) + ρ(C13—O)(5) + ν(C10—C16)(5)
783	777	772	769	770	770	–	R2[ν_{ring}](14) + ρ(CC17O)(11) + R2[δ_{ring}](8) + ρ(C16OO)(6) + ν(C—O6)(6) + ω(C=O8)(5) + δ(CO4C)(5)
767	761	763	755	–	–	–	oop(C=O8)(44) + R1[ν_{ring}](10) + ρ(C16OO)(9) + γ(C10—O)(6) + δ(CC16O)(5)
753	748	730	742	–	–	–	R2[δ_{ring}](15) + ρ(CC17O)(13) + δ(CO4C)(10) + ω(C=O9)(7) + ρ(C16OO)(6) + ρ(C13—O)(5)
746	741	720	732	733	740	–	oop(C=O9)(34) + R2[puck$_{ring}$](12) + ρ(CC17O)(7) + oop(C22—C19)(5) + ω(C19—H)(5) + oop(C13—H)(5)
712	705	705	698	–	–	–	ρ(C12O)(14) + R1[ν_{ring}](13) + δ(CC16O)(8) + R1[δ_{ring}](13) + R1[δ_{ring}](6) + ρ(C15H$_2$)(5)
705	670	696	692	–	–	–	R2[puck$_{ring}$](48) + oop(C—O7)(20) + ω(C20—O)(18)
670	665	604	674	677	–	–	oop(O3—H)((45) + ρ(CC17O)(14) + ρ(C13—O)(5)
649	644	602	593	–	–	–	oop(O3—H)((27) + ρ(CC17O)(11) + ρ(C13—O)(10) + ρ(C11O)(6) + R1[puck$_{ring}$](5) + R1[τ_{ring}](5)
609	604	598	590	–	–	604	R2[τ_{ring}](30) 8 oop(C22—C19)(26) + R2[puck$_{ring}$](14) + ω(C20—O)(11) + oop(C—O7)(5)
602	598	582	578	–	–	–	δ(CCO7)(22) + R2[δ_{ring}](18) + ρ(CC22C19)(13) + ρ(CC20O)(12) + R2[ν_{ring}](7) + ν(C—O6)(5) + δ(CC17O)(5)
594	590	549	567	–	–	–	R2[δ_{ring}](21) + R1[δ_{ring}](11) + R1[ν_{ring}](7) + δ(CC17O)(7) + δ(CC16O)(5) 8 δ(CC10—O)(5)
568	564	546	548	–	–	563	ρ(C10—O)(10) + ρ(C12O)(10) + R1[ν_{ring}](8) + ν(C10—C16)(7) + R1[δ_{ring}](7) + δ(CC10—O)(6) + ρ(C14H$_2$)(5) + R1[puck$_{ring}$](5)
547	543	522	523	–	–	–	ρ(C10—O)(31) + ρ(C16OO)(19) + ν(C10—O2)(5)ρ(C12O)(5) ν(C10—C16)(5)
529	525	517	515	–	–	–	δ(CC19C)(16) + R2[δ_{ring}](26) + ρ(CC17O)(12) + oop(O2—H)(5)
514	510	487	491	–	–	–	oop(O2—H)(65) + R2[δ_{ring}](5)
502	499	471	479	–	–	–	R2[δ_{ring}](16) + ρ(CC22C19)(8) + ρ(CC20O)(7) + ρ(C12O)(6)
475	471	466	475	–	–	–	oop(O7—H)(86) + oop(C—O7)(7)
466	462	443	452	–	–	–	R1[δ_{ring}](17) + ω(C11O)(9) + δ(CC17O)(8) + oop(O2—H)(7) + γ(C11O)(6) + ρ(CC20O)(5)
456	453	442	440	–	–	–	ω(C10—O)(12) + γ(C12O)(11) + γ(C13—O)(8) + oop(O1—H)(6) + ω(C12O)(5) + γ(C11O)(5)
444	441	417	431	–	–	–	R2[τ_{ring}]](31) + ω(C20—O)(23) + R2[τ_{ring}](18) + oop(C—O7)(10) + oop(O7—H)(7)
426	423	399	407	–	–	–	ω(C10—O)(8) + ρ(C10—O)(7) + γ(C13—O)(6) + R1[δ_{ring}](6) + δ(CC10—O)(6) + ω(C12O)(5) + δ(CC17O)(5)
398	395	393	401	–	–	–	oop(C—O7)(21) + R2[puck$_{ring}$](16) + ω(C20—O)(11) + oop(C22—C19)(7) + R2[oop(C24—H)](6) + R2[τ_{ring}](5)
394	391	388	394	–	–	–	R1[δ_{ring}](27) + δ(CC16O)(7) + ρ(C16OO)(5)
387	385	354	384	–	–	–	ρ(C10—O)(27) + δ(CC10—O)(15) + δ(CC16O)(14) + R1[puck$_{ring}$](10) + ν(C10—C16)(5) + R1[δ_{ring}](5)
365	362	340	343	–	–	–	R1[puck$_{ring}$](13) + γ(C12O)(8) + ω(C10—O)(7) + δ(CC10—O)(6) + δ(CO4C)(6) + R1[δ_{ring}](5) + R1[δ_{ring}](5) + R1[τ_{ring}](5)
331	318	312	314	–	–	–	oop(O1—H)(63) + τ(C—O5)(16) + R1[δ_{ring}](5)
320	328	332	314	–	–	–	oop(O1—H)(13) + δ(CCO7)(13) + R1[τ_{ring}](11) + ρ(CC20O)(6) + R1[puck$_{ring}$](6) + ρ(C13—O)(5)
314	311	308	290	–	–	–	ρ(CC20O)(24) + δ(CCO7)(22) + R1[τ_{ring}](8) + R1[δ_{ring}](6) + R2[δ_{ring}](6)
304	302	278	274	–	–	–	oop(C13—H)(15) + γ(C13—O)(12) + τ(O4—C17)(11) + R1[δ_{ring}](9) + ω(C10—O)(8) + δ(CO4C)(8) + γ(C10—O)(6)
304	302	261	268	–	–	–	oop(O1—H)(19) + ρ(C10—O)(17) + R1[puck$_{ring}$](13) + R1[τ_{ring}](6)
264	262	253	261	–	–	–	oop(C13—H)(19) + δ(CO4C)(8) + τ(O4—C17)(7) + γ(C13—O)(7) + δ(CC18C)(6) + R1[puck$_{ring}$](6) + γ(C11O)(5)
256	254	241	255	–	–	–	R2[τ_{ring}](27) + R2[oop(C23—H)](10) + ω(C20—O)(9) + τ(C17—C18)(8) + oop(C13—H)(7) + τ(C18—C19)(5)
252	250	229	246	–	–	–	R1[τ_{ring}](32) + R1[puck$_{ring}$](30) + γ(C10—O)(6) + oop(O1—H)(6)
228	227	228	233	–	–	–	oop(O6—H)(74) + oop(O7—H)(8) + R2[τ_{ring}](8)
227	225	221	216	–	–	–	γ(C10—O)(29) + R1[τ_{ring}](12) + δ(CO4C)(11) + ρ(CC17O)(5) + oop(O2—H)(5)
222	220	216	210	–	–	–	δ(CC17O)(18) + ρ(C13—O)(9) + ρ(CC22C19)(8) + δ(CO4C)(8) + ρ(CC17O)(7) + R1[δ_{ring}](7) + ρ(C10—O)(5)
195	194	201	192	–	–	–	R2[τ_{ring}](38) + R2[puck$_{ring}$](17) + τ(C17—C18)(12) + τ(C19—C22)(11) + oop(O6—H)(8) + oop(C22—C19)(5)
180	179	178	168	–	–	–	R1[δ_{ring}](22) + ρ(C11O)(11) + oop(O1—H)(10) + γ(C10—O)(6)
149	148	156	137	–	–	–	τ(C17—C18)(18) + R2[τ_{ring}](16) + τ(O4—C17)(15) + τ(C18—C19)(7) + γ(C13—O)(7) + τ(C19—C22)(6) + ω(C18—H)(6) + R1[τ_{ring}](5)
130	129	128	120	–	–	–	δ(CO4C)(19) + oop(C13—H)(12) + ρ(CC22C19)(8) + δ(CC19C)(7) + ν(C17—C18)(6) + δ(CC18C)(5) + R1[τ_{ring}](5)
102	101	112	99	–	–	–	R1[τ_{ring}](57) + τ(C—O5)(10) + oop(O1—H)(7) + τ(C10—C16)(7)
98	97	83	84	–	–	–	τ(C10—C16)(42) + τ(C—O5)(29) + oop(O1—H)(5) + oop(C13—H)(5)
81	80	73	76	–	–	–	τ(C10—C16)(20) + oop(C13—H)(17) + oop(O3—H)(12) + R1[τ_{ring}](7) + oop(C22—C19)(5)
74	73	59	69	–	–	–	τ(C10—C16)(47) + R1[τ_{ring}](19) + τ(C—O5)(8) + oop(O2—H)(8) + γ(C10—O)(5)
54	54	51	40	–	–	–	oop(C13—H)(53) + oop(O3—H)(15) + δ(CO4C)(5)
37	37	28	29	–	–	–	δ(CC18C)(18) + δ(CC17O)(18) + δ(CC19C)(14) + δ(CO4C)(10) + R1[τ_{ring}](7) + oop(O3—H)(5) + ρ(CC22C19)(5)
23	23	27	20	–	–	–	τ(O4—C17)(34) + oop(O3—H)(15) + τ(C18—C19)(10) + τ(C19—C22)(6) + oop(C13—H)(6) + γ(C13—O)(5)
20	19	21	16	–	–	–	oop(C13—H)(38) + τ(C19—C22)(18) + τ(C17—C18)(9) + τ(O4—C17)(8) + oop(O3—H)(7)

Proposed assignment and potential energy distribution (PED) for vibrational normal modes. Types of vibration: υ, stretching; δ, deformation; oop, out-of-plane bending; ω, wagging; γ, twisting; ρ, rocking; τ, torsion.

bonds. It also provides a convenient basis for the interpretation of hyperconjugative interaction and electron density charge transfer from the filled lone pair electrons. The second-order perturbation theory analysis of the Fock matrix in NBO basis of 3-CQA shows strong intramolecular hyperconjugative interactions. The NBO calculations have been carried out for the more stable conformer

3-CQA. The NBO analysis provides a description of the structure of a conformer by a set of localized bonds, anti-bonds, and Rydberg extra valence orbitals. Stabilizing interactions between filled and unoccupied orbitals, and destabilizing interactions between filled orbitals can also be obtained from this analysis [35]. The delocalization effects (or donor–acceptor CT) can be estimated from the presence of off-diagonal elements of the Fock matrix in the NBO basis. The second-order perturbation theory analysis of the Fock matrix in the NBO, basis of the 3-CQA molecule shows strong intramolecular hyperconjugative interactions which are presented in Table 2. The most important interaction (n–π^*) related to the resonance in the molecule is electron donation from the n2(O4) atom of the electron-donating group to the anti-bonding acceptor π^*(O9—C17) and results in a maximum stabilization energy of 44.90 kcal/mol. Some important interactions between Lewis and non-Lewis orbitals along with their interacting stabilization energies are presented in Table 2. The larger the $E^{(2)}$ value, the more intensive is the interaction between electron donors and acceptors, *i.e.* the stronger the electron donating tendency from electron donors to acceptors and the greater the extent of conjugation of the whole system are. There occurs a strong intramolecular hyperconjugative interaction of lone pair electrons from the O4 atom to the π^*(O9—C17) bond leading to a stabilization energy of 44.90 kcal/mol and from the O6 atom to the π^*(C20—C23) bond leading to a stabilization energy of 25.59 kcal/mol. These enhanced π^*(O9—C17) and π^*(C20—C23) NBOs further conjugate with π^*(C18—C19) and π^*(C22—C25), respectively. This results in enormous stabilization energies of 46.41 and 264.41 kcal/mol, respectively.

The intra-molecular hyperconjugative interactions are formed by the overlap between the π(C—C) and π^*(C—C) bond orbitals, which results in intra-molecular charge transfer (ICT) causing stabilization of the system. These interactions are observed as an increase in ED in the C—C anti-bonding orbital that weakens their respective bonds [36]. The ED at the four conjugated π bonds (~1.64–1.98e) and π^* bonds (~0.13–0.39e) of the molecule clearly demonstrates strong delocalization leading to the stabilization of energy in the range of 4.46–23.63 kcal/mol.

Vibrational analysis

The total number of atoms in the 3-CQA molecule is 43 resulting in 123 ($3N-6$) normal modes. Here, N is the number of atoms in the molecule. The calculated wavenumbers of the vibrational modes and potential energy distribution (PED) along the internal coordinates of the 3-CQA molecule, together with the observed wavenumbers are given in Table 3. Localized symmetry was used in the analysis of the PED obtained using the program GAR2PED [27]. PED values <10% have not been included in the table. The assignments of the infrared and Raman bands of 3-CQA are based on a comparison of the experimental spectra and theoretically obtained wavenumbers and PED values. This agreement is comparable to the one obtained by Biswas et al. [37].

DFT calculations yield Raman scattering amplitudes, which cannot be taken directly to be the Raman intensities. The Raman scattering cross sections, $\partial\sigma_j/\partial\Omega$, which are proportional to the Raman intensities may be calculated from the Raman scattering amplitude and predicted wavenumbers for each normal mode using the relationship [38,39]

$$\frac{\partial\sigma_j}{\partial\Omega} = \left(\frac{2^4\pi^4}{45}\right)\left(\frac{(v_0 - v_j)^4}{1-\exp\left[\frac{-hcv_j}{kT}\right]}\right)\left(\frac{h}{8\pi^2 c v_j}\right)S_j$$

where S_j and v_j are the scattering activities and the predicted wavenumbers, respectively of the jth normal mode, v_0 is the wavenumber of the Raman excitation line and h, c, and k are universal constants. The Raman intensities obtained using this relationship match quite nicely with the experimentally observed intensities as shown in Figs. 5 and 6.

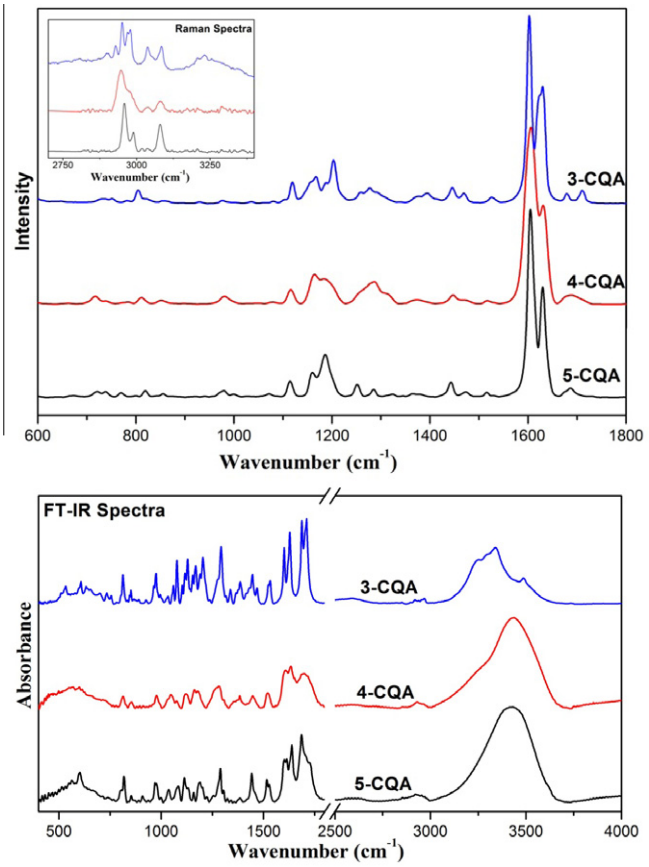

Fig. 5. Experimental Raman scattering and IR absorption spectra of 3-CQA, 4-CQA and 5-CQA.

The comparison of the wavenumbers calculated at B3LYP with the observed values (Table 3) reveals the over estimation of the calculated vibrational modes due to the neglect of anharmonicity found in the real system. The inclusion of electron correlation in DFT to a certain extent makes the wavenumber values smaller in comparison with the HF wavenumber data. In Table 3 a comparison of the wavenumbers of 3-CQA, 4-CQA, and 5-CQA molecules calculated at B3LYP is given. Experimental and calculated (scaled) Raman and IR spectra of 3-CQA, 4-CQA, and 5-CQA are shown in Figs. 5 and 6, respectively.

Phenyl ring vibrations

For the title compound 3-CQA the phenyl ring and cyclohexane ring vibrations are found to make a major contribution in the IR and Raman spectra of the sample. The calculations yielded the phenyl ring stretching vibrations at 1630, 1623, 1547, 1472, and 1415 cm^{-1}. These stretching vibrations are also present in 4-CQA and 5-CQA molecules in the same range.

Aromatic compounds commonly exhibit multiple weak bands in the region 3100–3000 cm^{-1} due to aromatic C—H stretching vibration [40]. In this region, the bands are not affected appreciably by the nature of the substituent. The 3-CQA has three C—H moieties. The phenyl ring vibrations assigned to the aromatic C—H stretch computed at 3092, 3071, and 3056 cm^{-1} by the B3LYP method are in good agreement with the recorded FT-Raman bands at 3108 and 3048 cm^{-1}. The bands observed at 937, 839, and

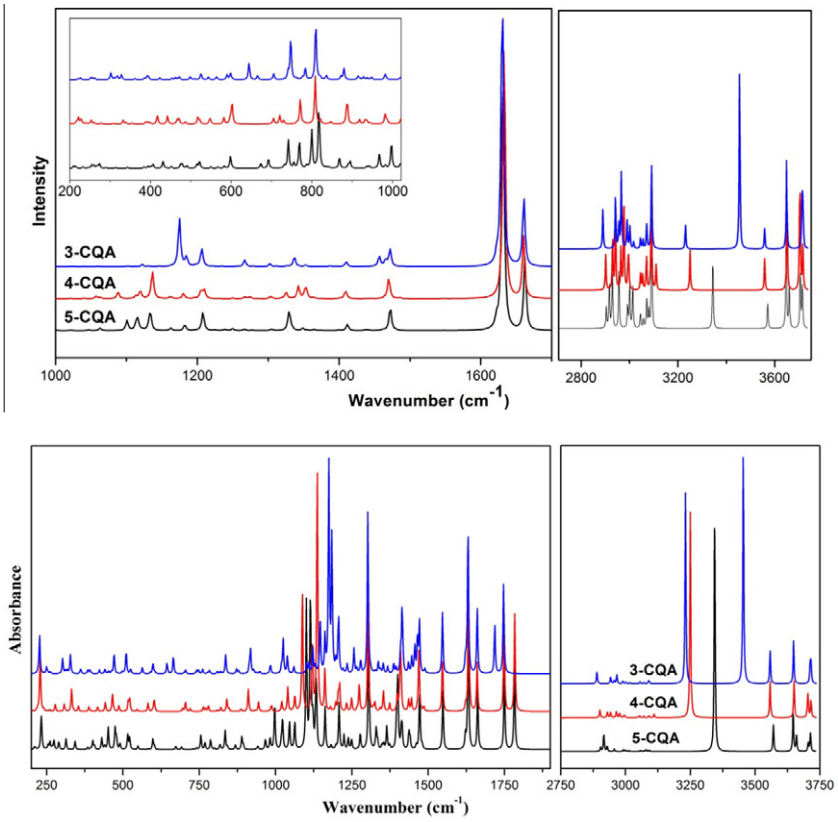

Fig. 6. Calculated (scaled) Raman scattering and IR absorption spectra of 3-CQA, 4-CQA and 5-CQA.

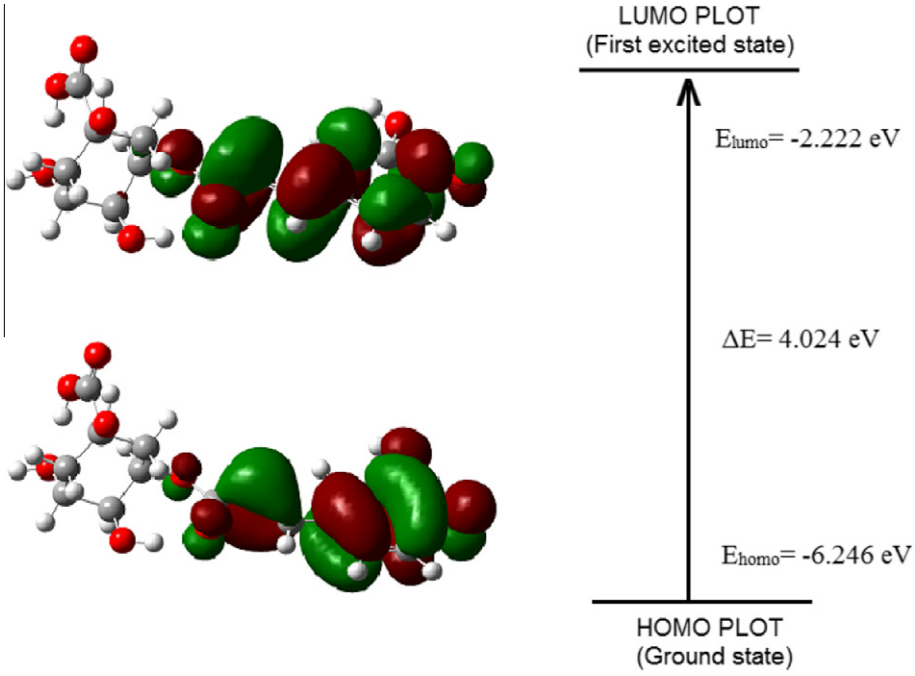

Fig. 7. Electron distribution of HOMO and LUMO energy levels for 3-CQA.

818 cm^{-1} in the IR are attributed to C—H out-of-plane bending vibrations of ring 2. These lines also show a good agreement with the theoretically scaled harmonic wavenumber values at 938, 837, and 820 cm^{-1}. The wavenumbers of torsions about the ring are calculated to be 604 and 441 cm^{-1} and match well with the observed values.

The molecule contains two CH_2 groups connected to the ring. The asymmetric CH_2 stretching vibrations are calculated to be 3017 and 3001 cm^{-1}. The symmetric CH_2 stretching modes are calculated to be 2956 and 2942 cm^{-1}, and can be assigned to the 2937 cm^{-1} band in the IR spectra. The CH_2 deformation modes are calculated to be 1489 and 1466 cm^{-1}, and a corresponding

Table 4
Thermodynamic properties of 3-CQA at different temperatures at B3LYP/6-311++G(d,p) level.

T (°K)	H_m (kcal/mol)	$C_{p,m}$ (cal/mol K)	S_m (cal/mol K)
100	212.181	34.604	97.089
200	217.079	62.949	131.287
300	224.728	89.836	162.74
400	234.968	114.37	192.6
500	247.465	134.852	220.845

peak is observed at 1487 cm^{-1} in the IR spectra. The CH_2 wagging modes are calculated to be 1368 and 1312 cm^{-1}.

Cyclohexane ring vibrations

The lines at 1102 and 1060 cm^{-1} are assigned to the cyclohexane ring stretching modes. The scaled vibrational modes computed in the range 3017–2890 cm^{-1}, correspond to the stretching modes of the C11—H, C12—H, and C13—H units. The wavenumbers of the asymmetric deformations of the ring are calculated to be 590 and 462 cm^{-1}; they have some shift with the experimental results. The trigonal deformation modes of the ring are calculated to be at 1109, 948, and 391 cm^{-1}. The asymmetric torsion modes are calculated to be at 250 and 101 cm^{-1}.

C-OH group vibrations

The characteristic peaks corresponding to the stretching modes of the OH groups are calculated at 3716, 3713, 3649, 3559, 3455, and 3231 cm^{-1}. The calculated wavenumbers for these modes in case of 4-CQA are 3716, 3705, 3703, 3651, 3558, and 3250 cm^{-1} and for 5-CQA are 3715, 3705, 3660, 3647, 3571, and 3344 cm^{-1}. These values differ much in all the conformers because of the different orientations of the aldehyde group. The C-OH in plane and out of plane bending modes are calculated in the region 1466–1344 cm^{-1}. The modes calculated at 1457, 1446 and 1415, 1410, and 1396 cm^{-1} are assigned to the COH bend.

Most of the characteristic features of the carboxylic group are observed usually in the region 1700–1800 cm^{-1}. High contributions of the C=O stretching band are calculated to be at 1719 and 1747 cm^{-1}. The C=O deformation modes are calculated to be at 761 and 741 cm^{-1}, which corresponds to a line at 733 cm^{-1} in the Raman spectrum. In the present work the C18—H and C19—H stretching vibrations are calculated at 3089 and 3045 cm^{-1}, respectively and are assigned to the strong peaks at 3080 and 3041 cm^{-1} in the Raman spectrum. The mixed vibrations originating from the C19H and C18H wagging modes are calculated to be at 1020 and 879 cm^{-1}.

Absorption spectra

The highest occupied molecular orbital (HOMO) and the lowest unoccupied molecular orbital (LUMO) are very important parameters for quantum chemistry. These orbitals are sometimes called the frontier orbitals, because they lie at the outermost boundaries of the electrons of the molecules. Both the HOMO and the LUMO are the main orbitals that take part in chemical stability [41]. The electronic absorption energies for all molecules were computed using time dependent density functional theory (TD-DFT). The atomic molecular orbital plots were obtained by Gauss View [15] and are sketched in Fig. 7. The energy gap between HOMO and LUMO is a critical parameter in determining molecular electrical transport properties because it is a measure of electron conductivity. The LUMO as an electron acceptor represents the ability to obtain an electron, and the HOMO represents the ability to donate an electron. Moreover, a smaller HOMO–LUMO energy gap explains the fact that eventual a charge transfer interaction is taking place within the molecule. The band gaps of 3-CQA, 4-CQA, and 5-CQA are 4.024, 4.083, and 4.004 eV, respectively. A comparison between the calculated band gaps of the 3-CQA, 4-CQA, and 5-CQA molecules show that 5-CQA is the most active molecule.

Thermodynamic properties

Thermal properties such as thermal diffusivities, specific heat capacities etc. of different forms of CQA are crucially important not only for the fundamental understanding of the molecules, but also for their processing and application. On the basis of vibrational analysis and statistical thermodynamics, the standard thermodynamic functions heat capacity ($C^{\circ}_{p,m}$), entropy (S°_{m}), and enthalpy (H°_{m}) were obtained and listed in Table 4. As observed from Table 4, values of heat capacity, entropy, and enthalpy all increase with the increase of temperature from 100 to 500 K, which is attributed to the enhancement of molecular vibrations while the temperature increases.

The correlation between these thermodynamic properties and temperatures T are shown in Fig. S1. The correlation equations for the tetramer of 3-CQA are as follows:

$$C^{\circ}_{p,m} = 2.7076 + 0.3294T - 1.29136 \times 10^{-4}T^2 \ (R^2 = 0.99989)$$

$$S^{\circ}_{m} = 61.5152 + 0.36668T - 9.64214 \times 10^{-5}T^2 \ (R^2 = 0.99998)$$

$$H^{\circ}_{m} = 209.6416 + 0.01222T + 1.27064 \times 10^{-4}T^2 \ (R^2 = 0.99997)$$

These equations could be used for further studies on the title compound. For instance, when the interaction of CQA with another compound is investigated, these thermodynamic properties could be obtained from the above equations and then could be used to calculate the change in Gibbs free energy of the reaction, which will help to judge the spontaneity of the reaction.

Conclusions

Geometry optimization using DFT at the B3LYP level with the extended basis set 6-311G(d,p) show that all the three isomers having very close energies. The equilibrium geometries and harmonic vibrational wavenumbers of all the 123 normal modes of the molecule were determined and analyzed investigating the most stable isomer of the chlorogenic acids (3-CQA). Raman and infrared spectra were recorded and the vibrational bands were assigned on the basis of the potential energy distribution obtained from the DFT calculations. The differences between the observed and scaled wavenumber values of most fundamentals are very small. Any discrepancy noted between the observed and the calculated wavenumbers is due to the fact that the calculations have been actually performed on a single (or isolated) molecule in the gaseous state while the experimental values had been recorded in the presence of intermolecular interactions. The HOMO–LUMO transition clearly explicates a charge transfer interaction in the whole molecular plane. The thermodynamic properties of 3-CQA at different temperatures were calculated, revealing the temperature dependence of $C^{\circ}_{p,m}$, S°_{m}, and H°_{m}. Information about the size, shape, charge density distribution, and site of chemical reactivity of the molecules has been obtained by mapping the electron density isosurface with ESP. We believe that our results will be a good starting point for studying the detailed potential surface of the 3-CQA and to understand the mechanism of 3-CQA molecule reactions in more detail in future.

Acknowledgements

The authors thank Prof. Nikolai Kuhnert and his coworkers for the HPLC–MS characterization of the samples. Bernd von der Kammer's help in preparing the samples is highly acknowledged. S.M. thanks the Indian Institute of Science Bangalore for providing the computing facilities, necessary to carry out the present work and Prof. S. Umapathy, Department of Inorganic and Physical Chemistry, Indian Institute of Science, Bangalore, for valuable suggestions.

Appendix A. Supplementary material

Supplementary data associated with this article can be found, in the online version, at http://dx.doi.org/10.1016/j.saa.2012.11.082.

References

[1] K. Herrmann, Crit. Rev. Food Sci. Nutr. 28 (1989) 315–347.
[2] C.A. Rice-Evans, N.J. Miller, G. Paganga, Free Radical Biol. Med. 20 (1996) 933–956.
[3] M. Stacewicz-Sapuntzakis, P.E. Bowen, E.A. Hussain, B.I. Damayanti-Wood, N.R. Farnsworth, Crit. Rev. Food Sci. Nutr. 41 (4) (2001) 251–286.
[4] M. Nardini, M. D'Aquino, G. Tomassi, V. Gentili, M. Di Felice, C. Scaccini, Free Radical Biol. Med. 19 (1995) 541–552.
[5] Y. Kono, K. Kobayashi, S. Tagawa, K. Adachi, A. Ueda, Y. Sawa, H. Shibata, Biochim. Biophys. Acta 1335 (1997) 335–342.
[6] H. Morishita, R. Kido, Assoc. Sci. Int. Cafe, Colloq. (1995) 119–124.
[7] M.R. Olthof, P.C.H. Hollman, M.B. Katan, J. Nutr. 131 (2001) 66–71.
[8] M.N. Clifford, J. Sci. Food Agric. 79 (1999) 362–372.
[9] C.A. Rice-Evans, N.J. Miller, G. Paganga, Free Radic. Biol. Med. 20 (1996) 933–956.
[10] C. Castelluccio, G. Paganga, N. Melikian, G.P. Bolwell, J. Pridham, J. Sampson, E.C. Rice, FEBS Lett. 368 (1995) 188–192.
[11] Y. Kono, H. Shibata, Y. Kodama, Y. Sawa, Biochem. J. 312 (1995) 947–953.
[12] H.G. Brittain, Spectroscopy 15 (2000) 44–49.
[13] P.J. Eravuchira, R.M. El-Abassy, S. Deshpande, M.F. Matei, S. Mishra, P. Tandon, N. Kuhnert, A. Materny, Vib. Spectrosc. 61 (2012) 10–16.
[14] M.J. Frisch, G.W. Trucks, H.B. Schlegel, G.E. Scuseria, M.A. Robb, J.R. Cheeseman, J.A. Montgomery, T. Vreven, K.N. Kudin, J.C. Burant, J.M. Millam, S.S. Iyengar, J. Tomasi, V. Barone, B. Mennucci, M. Cossi, G. Scalmani, N. Rega, G.A. Petersson, H. Nakatsuji, M. Hada, M. Ehara, K. Toyota, R. Fukuda, J. Hasegawa, M. Ishida, Nakajima, Y. Honda, O. Kitao, H. Nakai, M. Klene, X. Li, J.E. Knox, H.P. Hratchian, J.B. Cross, C. Adamo, J. Jaramillo, R. Gomperts, R.E. Stratmann, O. Yazyev, A.J. Austin, R. Cammi, C. Pomelli, J.W. Ochterski, P.Y. Ayala, K. Morokuma, G.A. Voth, P. Salvadorm, J.J. Dannenberg, V.G. Zakrzewski, S. Dapprich, A.D. Daniels, M.C. Strain, O. Farkas, D.K. Malick, A.D. Rabuck, K. Raghavachari, J.B. Foresman, J.V. Ortiz, Q. Cui, A.G. Baboul, S. Clifford, J. Cioslowski, B.B. Stefanov, G. Liu, A. Liashenko, P. Piskorz, I. Komaromi, R.L. Martin, D.J. Fox, T. Keith, M.A. Al-Laham, C.Y. Peng, A. Nanayakkara, M. Challacombe, P.M.W. Gill, B. Johnson, W. Chen, M.W. Wong, C. Gonzalez, J.A. Pople, Gaussian 03, Revision C.02, Gaussian, Inc., Wallingford, CT 06492, 2003.
[15] A. Frisch, A.B. Nielson, A.J. Holder, GAUSSVIEW User Manual, Gaussian Inc., Pittsburgh, PA, USA, 2000.
[16] C.T. Lee, W.T. Yang, R.G. Parr, Phys. Rev. B 37 (1988) 785–789.
[17] R.G. Parr, W. Yang, Density Functional Theory of Atoms and Molecules, Oxford University Press, New York, 1989.
[18] A.D. Becke, J. Chem. Phys. 98 (1993) 5648–5652.
[19] G.A. Petersson, M.A. Allaham, J. Chem. Phys. 94 (1991) 6081–6090.
[20] G.A. Petersson, A. Bennett, T.G. Tensfeldt, M.A. Allaham, W.A. Shirley, J. Mantzaris, J. Chem. Phys. 89 (1988) 2193–2218.
[21] A.K. Mishra, P. Tandon, J. Phys. Chem. 113 (44) (2009) 14629–14639.
[22] S. Mishra, D. Chaturvedi, A. Srivastava, P. Tandon, A.P. Ayala, H.W. Siesler, Vib. Spectrosc. 53 (2010) 112–116.
[23] M.D. Halls, J. Velkovski, H.B. Schlegel, Theor. Chem. Acc. 105 (2001) 413–421.
[24] S. Mishra, P. Tandon, A.P. Ayala, Spectrochim. Acta Part A 88 (2012) 116–123.
[25] P. Pulay, G. Fogarasi, F. Pang, J.E. Boggs, J. Am. Chem. Soc. 101 (1979) 2550–2560.
[26] G. Fogarasi, X. Zhou, P.W. Taylor, P. Pulay, J. Am. Chem. Soc. 114 (1992) 8191–8201.
[27] J.M.L. Martin, C. Van Alsenoy, Gar2ped, University of Antwerp, 1995.
[28] G.A. Zhurko, D.A. Zhurko, Chemcraft, 2005. <http://www.chemcraftprog.com>.
[29] A.E. Reed, L.A. Curtiss, F. Weinhold, Chem. Rev. 88 (1988) 899–926.
[30] J. Chocholousova, V. Vladimir Spirko, P. Hobza, Phys. Chem. Chem. Phys. 6 (2004) 22–37.
[31] J. Tomasi, in: P. Politzer, D. Truhlar (Eds.), Chemical Application of Atomic and Molecular Electrostatic Potentials, Plenum, New York, 1981, pp. 257–294.
[32] S. Moro, M. Bacilieri, C. Ferrari, G. Spalluto, Curr. Drug Discov. Technol. 2 (2005) 13–21.
[33] J.S. Murray, K. Sen, Molecular Electrostatic Ptentials, Concepts and Applications, Elsevier, Amsterdam, 1996.
[34] P.K. Weiner, R. Langridge, J.M. Blaney, R. Schaefer, P.A. Kollman, Electrostatic potential molecular surfaces, Proc. Natl. Acad. Sci. USA: Biophys. 79 (1982) 3754–3758.
[35] F. Weinhold, C.R. Landis, Valency and Bonding: A Natural Bond Orbital Donor Acceptor Perspective, Cambridge University Press, New York, 2005.
[36] C. James, G.R. Pettit, O.F. Nielsen, V.S. Jayakumar, I. Hubert Joe, Spectrochim. Acta 70A (2008) 1208–1216.
[37] N. Biswas, S. Kapoor, H.S. Mahal, T. Mukherjee, Chem. Phys. Lett. 444 (2007) 338–345.
[38] G.A. Guirgis, P. Klaboe, S. Shen, D.L. Powell, A. Gruodis, V. Aleksa, C.J. Nielsen, J. Tao, C. Zheng, J.R.J. Durig, J. Raman Spectrosc. 34 (2003) 322–336.
[39] P.L. Polavarapu, J. Phys. Chem. 94 (1990) 8106–8112.
[40] G. Varsanyi, Assignments for Vibrational Spectra of Seven Hundred Benzene Derivatives, vols. 1 and 2, Academiai Kiado, Budapest, 1973.
[41] S. Gunasekaran, R.A. Balaji, S. Kumaresan, G. Anand, S. Srinivasan, Can. J. Anal. Sci. Spectrosc. 53 (2008) 149–161.